Nanoscale

PAPER

View Article Online
View Journal | View Issue

Cite this: *Nanoscale*, 2025, **17**, 17285

An investigation into catalysed xanthene-based dye oxidation by a family of coordination cages†

James R. Williams and Michael D. Ward *

Received 30th May 2025,
Accepted 3rd July 2025

DOI: 10.1039/d5nr02293b

rsc.li/nanoscale

The ability of a family of $\mathbf{M_4}$, $\mathbf{M_8}$ and $\mathbf{M_{12}}$ coordination cages to effect catalytic oxidative degradation of a family of xanthene-based dyes using peroxymonosulfate (PMS) has been investigated in water. The $\mathbf{M_{12}}$ cages bind one dye molecule inside the central cavity; the $\mathbf{M_8}$ cages bind multiple anionic dye molecules around the external cage surface; the smallest $\mathbf{M_4}$ cages do not interact strongly with the dyes. Three separate sets of experiments showed that octanuclear $\mathbf{Co_8}$ was the most effective catalyst due to a combination of (i) its ability to bind multiple dye molecules around its surface in solution, and (ii) the Co(II)/Co(III) redox couple which activates the PMS anion by reducing it to the reactive species $SO_4^{\bullet-}$ close to the cage-bound substrates. Control experiments showed that replacing Co(II) by Fe(II), Ni(II) or Zn(II) in isostructural $\mathbf{M_8}$ cages removed catalytic activity, which specifically requires the Co(II)/Co(III) couple; and the effectiveness of the catalysis is guest-dependent according to parameters such as charge, hydrophobicity and inductive effect of substituents on the xanthene core. Overall the $\mathbf{Co_8}$ cage fulfils three functions of (i) binding the guest, (ii) activating the PMS using the Co(II)/Co(III) couple, and (iii) accumulating the $SO_4^{\bullet-}$ anions around the cationic cage surface close to bound guests.

Introduction

A particularly appealing application of coordination cage hosts is the catalysis of reactions of bound guests, a subject which has been extensively reviewed in recent years.[1] There are many mechanisms by which such catalysis can occur, including (but not limited to) (i) co-location of >1 reaction partners, meaning that each reactant experiences a high local concentration of the other; (ii) electrostatic factors whereby the high charge on a host cage can modify the affinity of a bound guest for protons, leading to substantial changes in acid- or base-catalysed reaction rates; (iii) constrictive binding, whereby folding a flexible guest in a confined space perturbs it towards the geometry of a transition state, thereby making it more accessible; and (iv) light-induced processes in which the host cage surrounding a guest incorporates light-harvesting chromophores or redox-active quenching groups in close proximity to the guest, facilitating reactions based on photoinduced electron transfer.[1]

Our recent work in this area, based on members of our family of coordinated cages that contain ditopic or tritopic ligands with pyrazolyl-pyridine chelating termini,[2] has made two distinct contributions. The first is that a range of catalysed reactions between hydrophobic organic guests and anions (which include hydroxide,[3a] enolates[3b] and phenolates[3c]) requires recognition of the anionic reaction partner at binding sites on the cationic cage surface: and these reactions can occur not just on cavity-bound substrates,[3] but also on substrates that are too large for the cavity but are nonetheless associated with the cage exterior surface *via* hydrophobic interactions.[4]

Our second recent contribution is that Co(II)-containing cages can act as redox partners for cage-catalysed oxidation reactions of substrates.[2b,5] Oxidants such as H_2O_2 and peroxymonosulfate, which are thermodynamically powerful but kinetically slow oxidants, may be activated by conversion to reactive oxygen species (ROS) using a low-potential $M^{n+}/M^{(n+1)+}$ redox couple in which the M^{n+} ion acts as a one-electron reducing agent.[6,7] If this happens using the Co(II) ions in the cage, then hydrophobic organic substrates that interact with the cage surface (exterior or interior) can be oxidised by the resulting high local concentration of reactive oxygen species, which will be further facilitated by the fact that anionic ROS will accumulate around the 16+ cage for electrostatic reasons. In these cases the cage therefore acts not only to co-locate substrate (organic substrate) and reaction partner (oxidant), but also [*via* the Co(II)/Co(III) couple] to activate the oxidant, thereby partici-

Department of Chemistry, University of Warwick, Coventry CV4 7AL, UK.
E-mail: m.d.ward@warwick.ac.uk

† Electronic supplementary information (ESI) available: All experimental details including synthesis/characterisation data for new compounds; details of spectroscopic and catalytic studies, and X-ray crystallography. CCDC 2455100–2455103. For ESI and crystallographic data in CIF or other electronic format see DOI: **https://doi.org/10.1039/d5nr02293b**

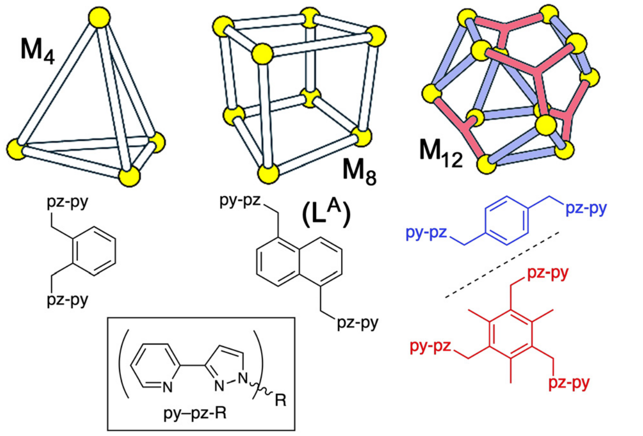

Fig. 1 Geometries of the M_4, M_8 and M_{12} cages, and the structural formulae of the associated ligands, used in this work.

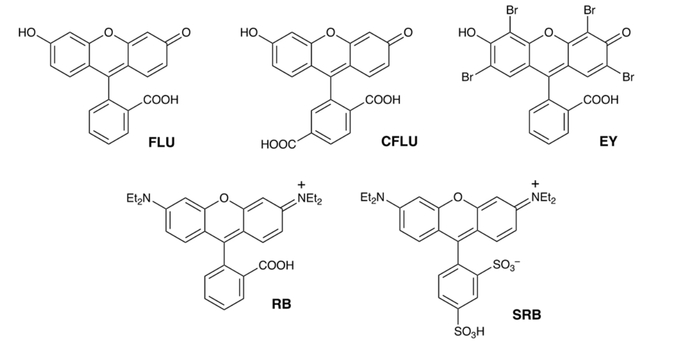

Fig. 2 Structures of the xanthene-based dyes used in this work.

pating directly in the reaction cycle and not just acting as a container.[5]

A specific example of this type of reactivity that we reported recently was the oxidation of xanthene-based dyes such as fluorescein with peroxymonosulfate (PMS), catalysed by the $\mathbf{Co_{12}}$ cage with a cuboctahedral geometry (Fig. 1);[5a] this cage contains four tritopic (face-capping) ligands and twelve ditopic (edge-bridging) ligands, and has an internal cavity volume of *ca.* 1100 Å^3.[8] We described the catalytic process as occurring through the encapsulation of a dye molecule inside the $\mathbf{Co_{12}}$ internal cavity, and generation of the reactive radical anion $SO_4^{\bullet-}$ by the redox reaction of PMS with Co(II) ions in the cage (eqn (1)).‡ The strong tendency of anionic species to accumulate round the cage surface[2–4] (the Co_{12} cage carries a 24+ charge) results in co-location of substrate and oxidant which is the source of the catalysis.

$$Co^{2+} + HSO_5 \rightarrow Co^{3+} + SO_4^{\bullet-} + HO^- \quad (1)$$

Significantly, control experiments conformed that *both* (i) binding of substrate by cage, and (ii) redox activity of the Co(II) ions, were essential. Replacing Co(II) ions with Zn(II) ions in an isostructural cage completely removed the catalytic effect. An equal number of mononuclear Co(II) complexes of similar redox potential – *i.e.* removing the possibility of a complete cage encapsulating the substrate – likewise removed most of the catalysis.[5a]

In this paper we report a more extensive study into the PMS-based oxidation of xanthene dyes catalysed by our octanuclear cubic $\mathbf{M_8}$ cages.[2c] The smaller size of these compared to the $\mathbf{M_{12}}$ cages means that interaction of the cages with the dyes is necessarily at the external surface as the dyes cannot fit inside the cavities. The $\mathbf{Co_8}$ cage has been shown to bind multiple equivalents of xanthene dyes such as fluorescein (**FLU**, Fig. 2) at the anion binding sites on each face exterior surface,[9] but cannot accommodate guests of that size inside the cavity. As part of this work we have also varied the metal ions used to include Fe(II) and Ni(II) to see the effect of having different metal ions (with different redox properties) on the catalysis which relies on initial activation of the PMS using the M(II)/M(III) couple.

Importantly, the use of dye molecules – of this class and many others – in industrial and large-scale processes is widespread. In many cases, these dyes are acutely toxic to aquatic life, meaning that waste water treatment for large scale processes is an ongoing problem.[10] Environmentally friendly oxidants used in advanced oxidation processes, whose activity is based on formation of reactive oxygen species, can result in complete destruction of the dye with only water and carbon dioxide produced from hydrocarbon dyes.[11] PMS has recently emerged as a more potent oxidant than hydrogen peroxide: like H_2O_2, it requires an initial redox-based activation step – often with a redox-active metal ion – to afford the reactive radical anion $SO_4^{\bullet-}$ as discussed above.[6,7] Accordingly this is a type of cage-based catalysis of potentially significant value and it may be extendable to other substrates that are susceptible to reaction with H_2O_2 or PMS and which bind to (or within) the host cage.

Results and discussion

Range of compounds used: cages, control complexes, and substrates

The cage complexes used in this investigation are presented in Fig. 1: these are cuboctahedral $\mathbf{Co_{12}}$,[8b] cubic $\mathbf{M_8}$ (M = Fe, Co, Ni, Zn)[2–4] and tetrahedral $\mathbf{Co_4}$ cages.[12] Of these, full synthesis/characterisation of $\mathbf{Fe_8}$ has not been reported before: it is prepared in the same way as the regularly-studied $\mathbf{Co_8}$ cage[2c] and relevant details are included in the ESI,† with the crystal structure of the new $\mathbf{Fe_8}$ cage being essentially identical to the structure of those with M = Co, Ni and Zn.

In addition simple mononuclear complexes $[M(pypz\text{-}Me)_3]^{2+}$ (denoted $\mathbf{M_1}$; M = Fe, Co, Ni, Zn, and based on a known ligand[13]) have been prepared (details in ESI†) to be used for control experiments and electrochemical studies,

‡ Note that $SO_4^{\bullet-}$ does not oxidise the ligands used in the cages. Xanthene dyes are particularly prone to oxidative degradation, hence their popularity for use as substrates to monitor efficacy of advanced oxidation process.[11]

based on the fact that the metal ions are in the same coordination environment as those in the larger cages: accordingly they should mimic the redox activity of metal ions in the cages, but without any ability to encapsulate guests. Given the inequivalence of the coordinating N atoms in the bidentate ligand pypz-Me, these mononuclear complexes are formed as a statistical (1 : 3) mixture of *fac* and *mer* isomers,[14] as clearly evident in some of the NMR spectra, and which precisely matches what happens during assembly of the $\mathbf{M_8}$ cubic cages which contain two *fac* tris-chelate and six *mer* tris-chelate vertices.[2a,14b] Consequently these mononuclear complexes are reasonable mimics of the metal vertices in the larger cages. Crystals of $[Co(pypz\text{-}Me)_3](BF_4)_2$ incorporate only the *mer* isomer: although one ligand is disordered over two orientations, both components are meridional (see ESI†). In crystals of $[Zn(pypz\text{-}Me)_3](BF_4)_2$ the positional disorder of ligands is more severe so this is not reported in full, we just note that it is isostructural with the Co(II) analogue and is clearly mononuclear $[Zn(pypz\text{-}Me)_3](BF_4)_2$.

The xanthene-based dyes used in this study (Fig. 2) are fluorescein (**FLU**), 6-carboxyfluorescein (**CFLU**), eosin-Y (**EY**), rhodamine-B (**RB**) and sulforhodamine-B (**SRB**). Both **FLU** and **EY** exist as dianions in neutral aqueous solution; **CFLU** with its extra carboxylic acid group can be a trianion. **RB** and **SRB** both contain an iminium group rendering **RB** neutral and zwitterionic in neutral solution; and **SRB** is anionic overall but with charge imbalance over the dye (a cationic iminium group, and two anionic sulfonate units). **FLU** and **EY** have both been studied in the investigation on the catalytic activity of the $\mathbf{Co_{12}}$ cage,[5a] and will therefore serve as points of comparison.

The range of cages, substrates and metal ions used allows for investigation of three variables. In this work we have:

• used a single dye substrate (**FLU**) but a range of different catalyst types containing 1, 4, 8 or 12 metal ions: what is the effect of catalyst structure/nuclearity on oxidative dye degradation?

• used a single cage ($\mathbf{Co_8}$) as catalyst to examine the effectiveness of the catalysed oxidations with different xanthene dye substrates: how do substrate properties such as charge and hydrophobicity affect catalysis?

• used a single cage type ($\mathbf{M_8}$) and single dye substrate (**FLU**) but varied the nature of the metal ion in the cage [Fe(II), Co(II), Ni(II), Zn(II)] to examine effect of metal ion redox properties on the cage-based catalysis.

Crystal structures of $\mathbf{M_8}$ cage/dye assemblies

To illustrate how the dye molecules can interact with the cage exterior surface, we crystallised samples of the $\mathbf{Ni_8}$ cage in the presence of $\mathbf{EY}^{2-}$ and $\mathbf{SRB}^{-}$ (as their sodium salts) and performed crystallographic analyses of the single crystals obtained in which the dye anions had replaced some of the tetrafluoroborate anions. Of course crystal structures may not replicate solution speciation but they are usefully illustrative.

The structure of $\mathbf{Ni_8{\cdot}EY}$ contains $\mathbf{EY}^{2-}$ anions in the lattice in spaces between cage complex cations, as these anions are too large to occupy the cage cavity. The $\mathbf{EY}^{2-}$ anions occupy two crystallographically different sites: this is illustrated in Fig. 3 in which the $\mathbf{EY}^{2-}$ anions are coloured red or purple to indicate the different crystal sites.

There are 1.7 $\mathbf{EY}^{2-}$ anions per $\mathbf{Ni_8}$ cage cation (which carries a charge of 16+), with the anions coloured red having a site occupancy of 1.0, and those in the alternate site (coloured purple) having a site occupancy of 0.7. This leaves 12.6 tetrafluoroborate anions required per cage to balance the charge, of which 10.45 could be accounted for during the refinement, with the balance likely being a casualty of the extensive disorder of anions/solvent molecules which required use of the solvent mask function to remove diffuse electron density that could not be modelled. As usual, some of the BF_4^- anions are associated with the windows in the centre of the cage faces where they are anchored by multiple CH⋯F hydrogen-bonding interactions (see ESI†). The $\mathbf{EY}^{2-}$ anions are positioned so as to lie close to and 'embracing' parts of the cage surface close to the Ni^{2+} ions, in the regions of highest positive electrostatic potential around the cage vertices, where there are multiple electrostatically-assisted supramolecular interactions (CH⋯π, π⋯π and CH⋯O) between cage surface and anions (Fig. 4).

Similar behaviour was observed in the $\mathbf{Ni_8{\cdot}SRB}$ complex (Fig. 5 and 6). The $\mathbf{SRB}^{-}$ anions are all crystallographically equivalent, with a site occupancy of 0.75; the asymmetric unit of the structure contains half of the cage (which lies across an

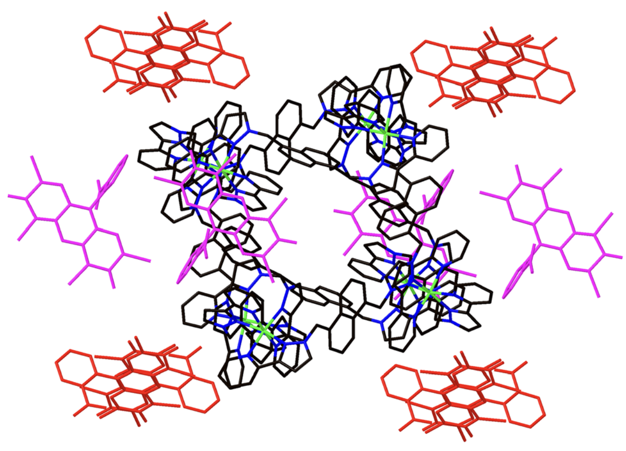

Fig. 3 View of the crystal structure of $\mathbf{Ni_8{\cdot}EY}$ with the two crystallographically inequivalent $\mathbf{EY}^{2-}$ molecules shown in different colours.

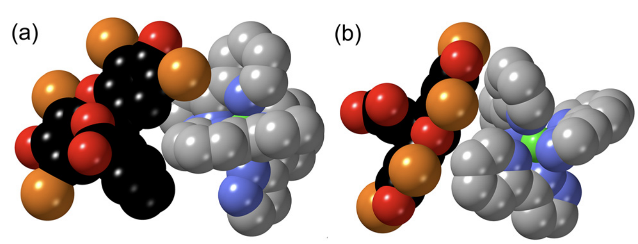

Fig. 4 Partial views of the structure of $\mathbf{Ni_8{\cdot}EY}$ showing the interactions of the anionic dye guests with the external surface of the cage around the vertices (orange spheres are the Br atoms).

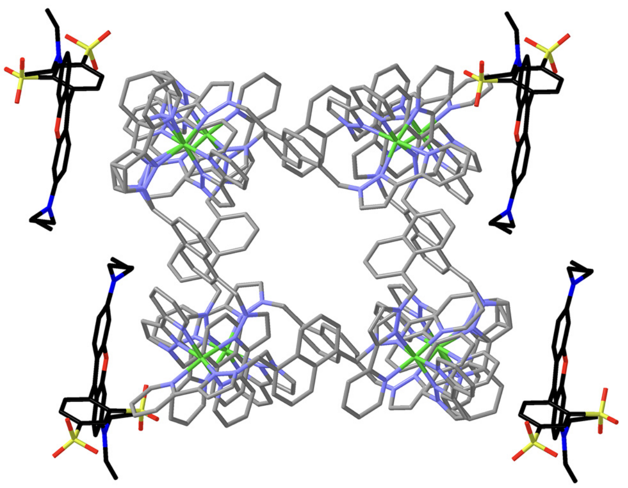

Fig. 5 View of the crystal structure of $\mathbf{Ni_8{\cdot}SRB}$ with the $\mathbf{SRB^-}$ anions shown in darker colours than the cage for emphasis (S atoms coloured yellow; O atoms coloured red).

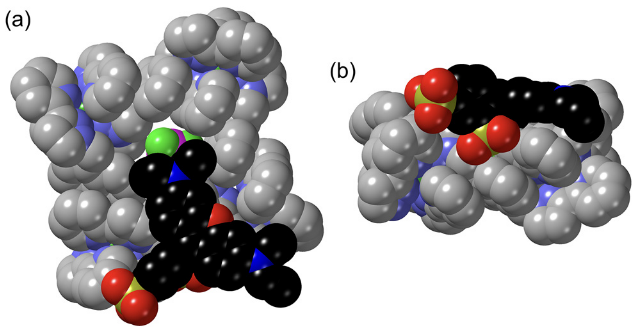

Fig. 6 Partial views of the structure of $\mathbf{Ni_8{\cdot}SRB}$ showing the interaction of the $\mathbf{SRB^-}$ dye guest with the external surface of the cage and a fluoroborate anion in one of the surface portals. View (a) is looking down onto one of the cage faces showing all of the $\mathbf{SRB^-}$ guest; (b) is edge-on to the $\mathbf{SRB^-}$ guest showing the contact between the sulfonate groups and the cationic cage surface.

inversion centre) as well as 0.75 $\mathbf{SRB^-}$ anions, such that the balance is 1.5 $\mathbf{SRB^-}$ anions per complete $\mathbf{Ni_8}$ cage. This means that there must be 14.5 fluoroborate anions of which 7.8 could be crystallographically located, with the balance again being a casualty of disorder/removal of diffuse electron density using a 'solvent mask' function.

As with the $\mathbf{Ni_8{\cdot}EY}$ structure, the conformation of the anion (substantial twist between the phenyl ring and the xanthene core) facilitates a variety of close contacts between $\mathbf{SRB^-}$ and the cage exterior surface, with the negatively-charged sulfonate groups in particular participating in multiple CH⋯O hydrogen-bonding interactions close to a cationic cage vertex, of which the shortest, between a methylene proton H(46F) and sulfonate O atom O(43G), is 2.17 Å. Conversely the cationic NEt_2^+ terminus of $\mathbf{SRB^-}$ lies over one the portals in the face centres, close to one of the surface-bound tetrafluoroborate anions, such that there is evidence for weak CH⋯F interactions between an NEt_2^+ terminus of the dye and BF_4^- [separations of C(27G) from F(13X) and F(15X) are 3.52 and 3.49 Å respectively]. This combination of interactions between $\mathbf{SRB^-}$, the cage vertices, and the portal-bound anion results in the $\mathbf{SRB^-}$ anion lying relatively flat to the cage surface, see Fig. 6. We have shown in recent work how such close cage/dye interactions can facilitate fast photoinduced electron transfer between a dye donor (**EY**) that is bound to a $\mathbf{M_8}$ cage exterior surface, and a naphthoquinone acceptor that is bound in the cage interior cavity.[15]

Effect of cage catalyst: catalysis of fluorescein oxidation using different $\mathbf{Co}_n$-based cage sizes (n = 0, 1, 4, 8, 12)

In our earlier initial work on redox-based catalysis, we established that $\mathbf{FLU^{2-}}$ underwent complete oxidative decomposition in minutes using the $\mathbf{Co_{12}}$ cage as catalyst in aqueous solution with PMS as oxidant, which was facilitated by strong ($\log K$ = 6.7) 1 : 1 cage : guest binding; a stoichiometry which suggests that the $\mathbf{FLU^{2-}}$ substrate could bind *inside* the $\mathbf{Co_{12}}$ cage cavity.[5a] Accordingly we were interested to see how this compared with catalysis by the smaller $\mathbf{Co_8}$, $\mathbf{Co_4}$ and $\mathbf{Co_1}$ complexes under the same conditions. We also know from earlier work that the $\mathbf{Co_8}$ cage has the capacity to bind multiple anionic dye molecules of this general type around its external surface:[9] this binding is strong due to a combination of the negative charge on the dye molecules, and their large hydrophobic surface area, with (for example) a 1 : 1 binding constant between **FLU** and $\mathbf{Co_8}$ of 1×10^5 M^{-1}.§ As **FLU** is too large to bind as a guest inside the smaller cavity of $\mathbf{Co_8}$ (compared to $\mathbf{Co_{12}}$) this binding has to be association with the *external* surface, in a way that we routinely see with smaller anions that occupy the windows in the $\mathbf{M_8}$ cage surfaces.[2a,16] Further support for this came from a Job plot experiment which showed that several **FLU** anions could bind to the surface of each $\mathbf{Co_8}$ cage (*ca.* 5 : 1, with similarly large values for related dye molecules) when the molar ratio of components was optimised for this: a stoichiometry completely incompatible with cavity binding, which suggests that in solution that the anionic dye molecules can associate with each face of the cubic cage.[9]¶

§ We note that the conditions under which the fluorescence quenching titrations are done – with a substantial molar excess of Co_8 beyond the early stages of the titration – means that guest molecules will be distributed across an excess of Co_8 host molecules, such that fitting the curves to a 1 : 1 cage : guest stoichiometry is justified, even if aggregates with different ratios are possible early in the titration when the substrate is in excess (*cf.* Job plots); accordingly we only quote the 1 : 1 binding constants to one significant figure.

¶ In this new work the conditions for measuring binding constants are slightly different from what was used in ref. 9 (solvent is 2% dmso/98% water rather than pure water, to facilitate solubility of some of the cage catalysts, and there are no substituents on the exterior of this $\mathbf{Co_8}$ cage): but we checked that the dye/cage binding is essentially unchanged. We confirmed strong binding for the $\mathbf{FLU/Co_8}$ combination ($K = 1 \times 10^5$ M^{-1} for the 1 : 1 binding constant, as before) based on a fluorescence titration: and a Job plot experiment again confirmed the possibility for multiple **FLU** dye units to aggregate around the cage surface, with a maximum at a $\mathbf{FLU : Co_8}$ ratio of *ca.* 4 : 1 being possible even at the low concentrations used (see ESI†).

In contrast we found no such strong interaction between **FLU** and the smaller **Co$_4$** cage: a fluorescence-based titration of **Co$_4$** into a solution of **FLU**, under the same conditions as used for **Co$_{12}$** and **Co$_8$** (10^{-5} M concentration domain in 2% dmso/98% aqueous buffer) showed very little quenching of **FLU** by **Co$_4$**, indicative of a much weaker **Co$_4$**/**FLU** interaction. We suggest on the basis of this that strong binding of **FLU** to **Co$_{12}$** is driven by 1 : 1 cavity binding; strong binding of **FLU** to **Co$_8$** is driven by association with the external surfaces where the portals provide good H-bond donor sites to anionic guests; but as **Co$_4$** possesses neither of the necessary structural features to bind **FLU** strongly (neither a significantly-sized central cavity to encapsulate the guest, nor surface windows to provide a convergent H-bond donor site) the **Co$_4$**/**FLU** association is insignificant in this solvent at the concentrations used.

Armed with this knowledge of relative affinities we can understand the data in Fig. 7, which shows graphs plotting disappearance of the absorption maximum of **FLU** at 489 nm as a function of time, at concentrations of **Co$_{12}$**, **Co$_8$**, **Co$_4$** and **Co$_1$** catalysts as required to give the same total concentration of Co(II) ions for the redox activation of PMS which is the ultimate oxidant. There are some obvious conclusions that we can draw from this based on knowledge of cage/guest binding behaviour. Firstly, in the absence of any Co(II) complex as catalyst, oxidation of **FLU** by PMS is very slow due to the lack of redox activation (dotted line). The mononuclear complex **Co$_1$** provides some redox activation: the catalysis associated with this (green line) cannot involve any kind of guest encapsulation in a cage, but it is likely that some modest degree of **FLU^{2-}**/**Co$_1$** association can occur for electrostatic reasons to bring the substrate close to where the $SO_4^{\bullet-}$ ions are generated. The **Co$_4$** cage performs similarly to **Co$_1$** as a catalyst [for the same overall concentration of Co(II) ions]: the reaction rate is slightly faster at early times (steeper gradient of the purple line compared to green in Fig. 7) and tails off later. Given the lack of a strong interaction between **Co$_4$** and **FLU** this general lack of any improved catalysis by **Co$_4$** compared to **Co$_1$** for the same concentration of Co(II) ions makes sense. Then we see better catalysis and faster oxidative destruction of **FLU^{2-}** by **Co$_{12}$**, as we reported earlier, based on strong 1 : 1 cage : guest binding involving cavity encapsulation.[5a] Finally – the most interesting observation – we see that the **Co$_8$** cage is a substantially more effective catalyst than **Co$_{12}$** with an initial reaction rate that is ≈3 times higher for the same overall Co(II) ion concentration. We attribute this to the ability of the **Co$_8$** cage to bind multiple **FLU^{2-}** guests around the exterior surface, at the anion binding sites on the faces, as the Job plot experiment demonstrate (ref. 9 and ESI†): this provides the possibility for each **Co$_8$** cage to assemble multiple substrates in the vicinity of the Co(II) ions where redox activation of PMS is occurring and the reactive $SO_4^{\bullet-}$ species are generated. In the early stages of these reactions, plots of ln[**FLU**] *vs.* time show a linear decrease indicating a reaction that is first-order in substrate (see ESI†); the derived reaction rate constants are in Table 1, and it is clear that **Co$_8$** stands out having both the fastest initial rate as well as the reaction proceeding furthest in the time window studied (Fig. 7) and is therefore the most effective catalyst for redox-based oxidative degradation of dyes of this type.

Effect of substrate: catalysis of oxidation of different dyes using the same Co$_8$ cage

Given that the cubic **Co$_8$** cage is clearly the best catalyst for this reaction type from the series **Co$_1$**/**Co$_4$**/**Co$_8$**/**Co$_{12}$** (Fig. 7), we next extended the study on oxidative dye degradation to a broader set of substrates shown above but using the same **Co$_8$** catalyst in each case, with the aim now of looking at effects of differences in substrate structure. The binding behaviour of **FLU**, **CFLU** and **EY** with a closely-related **Co$_8$** cage was reported in detail earlier,[9]¶ but **RB** and **SRB** have not been investigated before in this context. Fluorescence quenching titrations per-

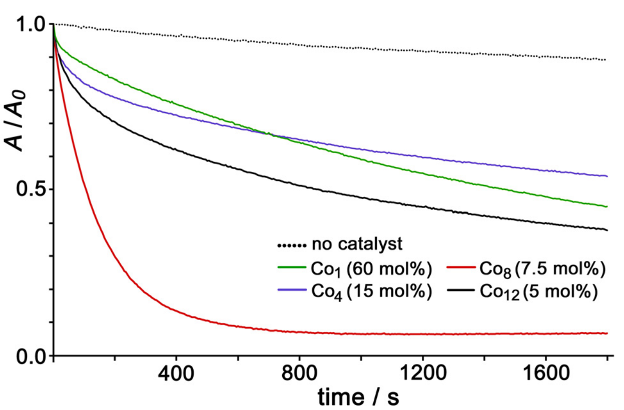

Fig. 7 Normalised UV/vis absorption data showing destruction of **FLU** (7.5 μM, λ_{max} = 489 nm) by oxidation with PMS (45 eq.) over time with no catalyst, **Co$_{12}$** (5 mol%), **Co$_8$** (7.5 mol%), **Co$_4$** (15 mol%) and **Co$_1$** (60 mol%), with cage concentrations adjusted to give the same concentration of Co(II) centres in each case. Solvent was aqueous buffer containing TWEEN-20 surfactant (see ref. 5a) at pH 7.

Table 1 First order reaction rate constants for dye degradation reactions based on initial rate data from first 100 seconds using experimental data shown in Fig. 7 and 8[a,b]

Catalyst	Substrate	Background,[c] 10^4k/s^{-1}	Catalysed,[d] 10^4k/s^{-1}	Relative increase
Co$_1$	**FLU**	1.05	11.1	10.6
Co$_4$	**FLU**	1.05	16.6	15.8
Co$_8$	**FLU**	1.05	64.8	61.7
Co$_{12}$	**FLU**	1.05	23.9	22.8
Co$_8$	**CFLU**	6.03	83.4	13.8
Co$_8$	**EY**	2.09	26.2	12.5
Co$_8$	**RB**	12.2	59.6	4.9
Co$_8$	**SRB**	20.4	121	5.9

[a] Conditions are given in captions to Fig. 7 and 8 [7.5 μM substrate, 45 eq. PMS, catalyst loadings varied as indicated to give same concentration of Co(II) units]. [b] Rate constants can be converted to second-order on dividing by catalyst concentration, but to facilitate comparison for the same Co(II) ion concentration they have been left as first order. [c] Rate for dye degradation in presence of PMS but with no metal complex catalyst present. [d] Background reaction rate subtracted in each case.

formed by adding portions of $\mathbf{Co_8}$ to samples of these dyes afforded binding constants (using Bindfit)[17] of 5×10^4 M^{-1} for **RB** and 7×10^4 M^{-1} for **SRB**, both slightly smaller than what we measured with **FLU**, possibly for simple electrostatic reasons given their smaller negative charges (0 and −1 respectively). The hydrophobicity of the xanthene dye is a significant additional factor in driving association with $\mathbf{Co_8}$,[9] as we have reported before with a range of different guest types,[2–4] including diacetyl-fluorescein which bound strongly to the external surface of a $\mathbf{Co_8}$ cage despite being neutral.[4b] Job plots to investigate the stoichiometry of possible aggregates between $\mathbf{Co_8}$ and the dyes **RB** and $\mathbf{SRB^-}$ confirm that, as observed earlier with **FLU**, **CFLU** and **EY**, multiple dye units can accumulate around the $\mathbf{Co_8}$ cage surface under different mole fraction conditions (see ESI for examples†).

Fig. 8 shows the time-dependent oxidative destruction of the five different dye substrates using PMS as oxidant with $\mathbf{Co_8}$ as catalyst. In all cases there is an obvious and substantial increase in reaction rate in the presence of $\mathbf{Co_8}$ compared to the much slower reactions in its absence (see for example Fig. 7, dotted line). Again the early-time kinetic data is first order in substrate (see ESI†): after subtraction of the uncatalysed background reaction rates (absence of $\mathbf{Co_8}$) in each case we find initial rate accelerations compared to background spanning the range of factors from 5 (for **RB** and **SRB**) to 62 (for **FLU**), see Table 1. Notably from Fig. 8 we can see that destruction of **FLU**, **CFLU** and **SRB** approaches completion fairly quickly, within *ca.* 600 seconds, whereas destruction of **EY** and **RB** tails off more slowly with substantial amounts of unreacted substrate remaining even after 2000 seconds.

This variation in extent and rate of reaction with different substrates is interesting as it does not simply relate to any one obvious parameter like guest charge. The least effective catalysis, in terms of the extent of reaction which is <50% complete after 30 minutes, is with the substrate **EY**: which might suggest that electrostatic repulsion between the substrate (2− charge) and the reactive species $SO_4^{\bullet-}$ slows down the reaction. However the other dianionic substrate **FLU** reacts significantly faster, and also shows the greatest increase relative to the background reaction, which undermines that suggestion.

A factor here could be that as the reaction is an exhaustive oxidation of the dye, the electron-withdrawing Br atom substituents on **EY** make the xanthene core more resistant to oxidation. Whilst the ground-state redox potentials for the *first* oxidation of **FLU** and **EY** are similar to one another,[18] this is because they are localised in each case on the benzoate unit which is pendant from the xanthene core and orthogonal to it, such that the Br substituents have little electronic effect.[18b] However, subsequent oxidations of the xanthene unit will necessarily be affected by the electron-withdrawing effects of the Br substituents which are well known to make redox potentials more positive, *cf.* the simple example of the series ferrocene, bromoferrocene and 1,1′-dibromoferrocene whose Fe(II)/Fe(III) couples occur at +0.45, +0.63 and +0.76 V respectively in MeCN *vs.* Ag/AgCl.[19] This effect plausibly accounts for **EY** being the least reactive substrate in this set of experiments.

SRB is the substrate which shows the most complete reaction, with >95% dye destruction after <10 minutes, possibly because the presence of only a single negative charge results in less electrostatic repulsion with $SO_4^{\bullet-}$ than was the case with the dianionic substrates, though **SRB** also had the highest uncatalysed reaction rate. If we believe that $SO_4^{\bullet-}$/substrate electrostatic repulsion has a significant effect, then by that logic neutral **RB** should show the best catalysis: but this is clearly not the case, and we note that **RB** has the weakest binding to $\mathbf{Co_8}$ of the whole set, so will have the smallest proportion of any of the substrates brought into the reaction zone around the cage surface of any of the substrates under the conditions used.

Thus, inductive effects of substituents, and binding constant of the dye to the catalyst (which in turn relates to charge and hydrophobicity),[9] all play a role in determining the relative reactivity of the different substrates with a given catalyst: with the substrate that stands out most being **EY** with its resistance to oxidation arising from the electron-withdrawing Br substituents.

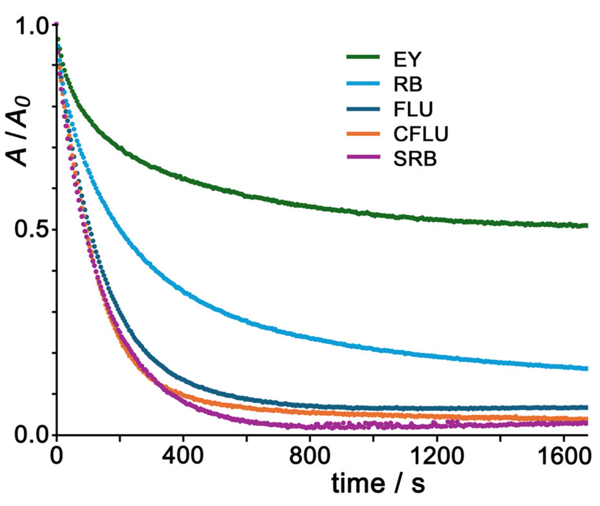

Fig. 8 Normalised UV/vis absorption data for the relevant dye maxima showing the destruction of **FLU**, **CFLU**, **EY**, **RB** and **SRB** (7.5 μM in each case) with PMS (45 eq.) over time with $\mathbf{Co_8}$ as catalyst, at 7.5 mol% catalyst loading. Solvent was aqueous buffer containing TWEEN-20 surfactant (see ref. 5a) at pH 7.

Effect of different metal ions in isostructural $\mathbf{M_8}$ cage catalysts

Given the obvious effectiveness of $\mathbf{Co_8}$ as a catalyst for this oxidative degradation reaction using PMS, and the fact that it requires the Co(II)/Co(III) redox activity of the metal ions in the cage to convert PMS to $SO_4^{\bullet-}$, the last variable we considered is the nature of the metal ion. Accordingly, we prepared the isostructural $\mathbf{Fe_8}$/$\mathbf{Ni_8}$/$\mathbf{Zn_8}$ cages to accompany the $\mathbf{Co_8}$ cage [Cu(II) does not form a similar cage structure]. Of these $\mathbf{Fe_8}$ is new but isostructural with the others (see ESI†). The effectiveness of the catalysis as the metal ion is varied across the isostructural cage series is shown in Fig. 9.

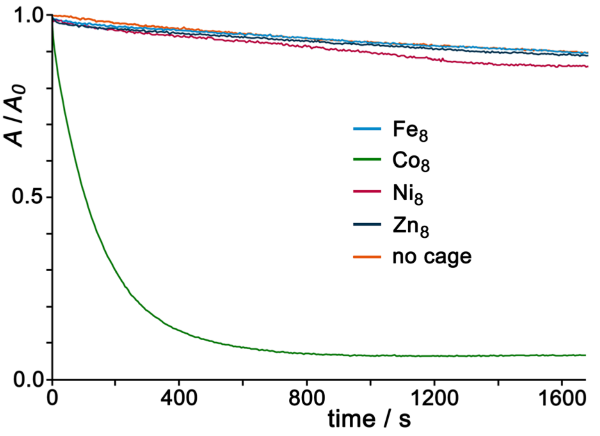

Fig. 9 Normalised UV/vis absorption data showing the destruction of FLU (7.5 uM, λ_{max} = 489 nm) with PMS (45 eq.) over time with no catalyst, $\mathbf{Co_8}$, $\mathbf{Fe_8}$, $\mathbf{Ni_8}$ and $\mathbf{Zn_8}$, all at 7.5 mol% catalyst loading. Solvent was aqueous buffer containing TWEEN-20 surfactant (see ref. 5a) at pH 7.

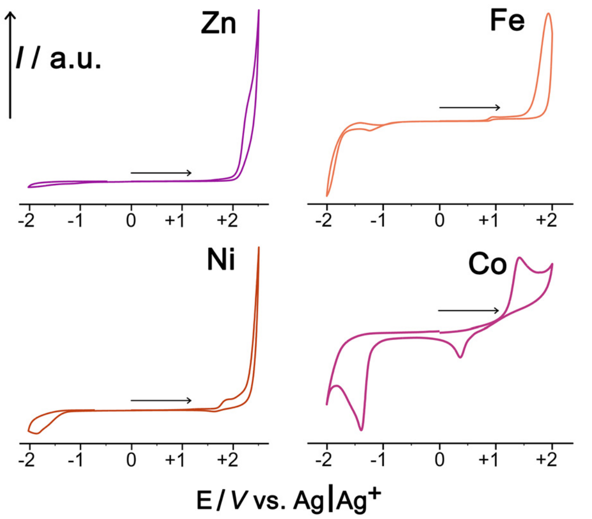

Fig. 10 Cyclic voltammograms of the $\mathbf{M_1}$ complexes (M = Fe, Co, Ni, Zn) in MeCN/0.1M TBAPF$_6$ at a scan rate of 0.1 V sec^{-1} using a boron-doped diamond working electrode, Pt wire counter-electrode, and an Ag/Ag$^+$ reference electrode. The horizontal arrows show the initial potential sweep directions.

The results are striking. We would not expect any catalytic activity from $\mathbf{Zn_8}$ compared to the absence of cage, given the impossibility of Zn(II)/Zn(III) redox activity, and indeed there is none: but $\mathbf{Fe_8}$ behaves similarly. $\mathbf{Ni_8}$ affords very slightly higher reactivity after a long period than background but the effect is tiny. $\mathbf{Co_8}$ stands out amongst this isostructural series as being a uniquely effective catalyst for this reaction, and that must be because (i) the Co(II)/Co(III) redox process occurs at a potential which aligns with what is required to activate PMS *via* a one-electron reduction (eqn (1)), and (ii) it is reversible, allowing for multiple redox cycles.

To check this we measured cyclic voltammograms of the mononuclear model complexes $\mathbf{Fe_1}$, $\mathbf{Co_1}$, $\mathbf{Ni_1}$ and $\mathbf{Zn_1}$ in MeCN: this is a convenient solvent for simple electrochemical studies given its high potential window, and the redox potentials of metal-centred redox processes are not expected to be significantly solvent dependent when the metal ions are coordinatively saturated. As these mononuclear complexes contain the metal ions in the same coordination environment that exists at the $\mathbf{M_8}$ cage vertices, down to the 3 : 1 mix of *fac* and *mer* isomers,[14] this experiment provides a convenient basis for comparison between this set of metal ions. The CVs are shown in Fig. 10.

The Zn(II) complex, as expected, shows no redox activity at modest potentials and can therefore be used as a baseline for comparison purposes. The Ni(II) complex shows an additional non-reversible wave at *ca.* +1.8 V *vs.* Ag/Ag$^+$ which means that Ni(II) in this complex is not an effective reductant. The Fe(II) complex shows a very low-intensity wave around +1 V which can be tentatively ascribed to an impurity given how weak it is: the obvious main oxidation process, which is fully irreversible due to the absence of any return wave, occurs at *ca.* +1.8 V *vs.* Ag/Ag$^+$. The Co(II) complex behaves distinctly differently with an oxidation wave at *ca.* +1.5 V that is accompanied by a return wave at *ca.* 0.5 V; we ascribe this pair to a chemically reversible but electrochemically irreversible Co(II)/Co(III) process, with the large additional wave at −1.4 V *vs.* Ag/Ag$^+$ possibly being an irreversible Co(II)/Co(I) process. Thus $\mathbf{Co_1}$ differs from the other complexes in having a lower M(II)/M(III) redox potential (*i.e.* the M^{2+} ion is a better reductant for activation of PMS according to eqn (1)), and it also has the chemical reversibility which is essential for multiple redox cycles and catalytic turnover.

Finally, the obvious question arises as to how the catalytic cycle is completed by reduction of Co(III) back to Co(II). PMS oxidation is mechanistically complex and can generate multiple by-products including peroxide and superoxide,[21] both of which are capable of acting as reducing agents (generating O_2), which could plausibly provide a basis for completing the catalytic cycle.[5b]

Conclusions

This study has demonstrated the factors behind the effectiveness of members of our Co(II)-based coordination cage family at acting as catalysts for the peroxy-monosulfate based oxidative degradation of a range of xanthene dyes. These factors are (i) association of the dye 'guests' with the cage, either internally ($\mathbf{Co_{12}}$ cage) or at the exterior surface ($\mathbf{Co_8}$ cage); (ii) the ability of the Co(II)/Co(III) couple provided by the metal ions in the cage superstructure to activate PMS by converting it to the reactive species $SO_4^{\bullet-}$; and (iii) the fact that the $SO_4^{\bullet-}$ anions, which are not only generated at the cage surface but also held close to it by the high positive charge of the cage, will therefore be clustered around the bound dye molecule guests. The cage therefore performs the multiple functions of attracting substrates, generating the anionic reaction partner using a reversible cage-based redox process, and holding substrate and reaction partner in close proximity to effect the catalysis.

It is worth emphasising that this aligns with conceptually related examples of the use of coordination cages in photoredox catalysis which combine guest binding by a cage; incorporation of a photosensitising unit into the cage/guest assembly; and (as here) redox activity of components of the cage superstructure, often metal ions.[20] The $\mathbf{Co_8}$ cage is the most effective catalyst of this cage family for the PMS-catalysed oxidative degradation reactions under investigation, due in particular to its ability to bind multiple anions around the exterior surface. These results suggest multiple new avenues of study for use of coordination cages in supramolecular catalysis.

Author contributions

J. R. W. performed all experimental work (synthesis, catalysis, crystallography). M. D. W. conceived and supervised the project. Both authors contributed to the data analysis and manuscript preparation.

Conflicts of interest

There are no conflicts to declare.

Data availability

The data supporting this article have been uploaded as part of the ESI.†

Acknowledgements

We thank the University of Warwick for financial support, and Ms. Anjali John and Prof. Julie MacPherson for assistance with recording cyclic voltammograms.

References

1 (*a*) H. Vardhan, M. Yusubov and F. Verpoort, *Coord. Chem. Rev.*, 2016, **306**, 171; (*b*) E. G. Percástegui, T. K. Ronson and J. R. Nitschke, *Chem. Rev.*, 2020, **120**, 13480; (*c*) Y. Fang, J. A. Powell, E. Li, Q. Wang, Z. Perry, A. Kirchon, X. Yang, Z. Xiao, C. Zhu, L. Zhang, F. Huang and H.-C. Zhou, *Chem. Soc. Rev.*, 2019, **48**, 4707; (*d*) C. J. Brown, F. D. Toste, R. G. Bergman and K. N. Raymond, *Chem. Rev.*, 2015, **115**, 3012; (*e*) M. Yoshizawa, J. K. Klosterman and M. Fujita, *Angew. Chem., Int. Ed.*, 2009, **48**, 3418; (*f*) M. Otte, *ACS Catal.*, 2016, **6**, 6491; (*g*) C. M. Hong, R. G. Bergman, K. N. Raymond and F. D. Toste, *Acc. Chem. Res.*, 2018, **51**, 2447; (*h*) W.-X. Gao, H.-N. Zhang and G.-X. Jin, *Coord. Chem. Rev.*, 2019, **386**, 69; (*i*) L. Zhao, X. Jing, X. Li, X. Guo, L. Zeng, C. He and C. Duan, *Coord. Chem. Rev.*, 2019, **378**, 151; (*j*) M. Morimoto, S. M. Bierschenk, K. T. Xia, R. G. Bergman, K. N. Raymond and F. D. Toste, *Nat. Catal.*, 2020, **3**, 969; (*k*) T. Piskorz, V. Martí-Centelles, R. L. Spicer, F. Duarte and P. J. Lusby, *Chem. Sci.*, 2023, **14**, 11300; (*l*) Y. Jin, Q. Zhang, Y. Zhang and C. Duan, *Chem. Soc. Rev.*, 2020, **49**, 5561.

2 (*a*) M. D. Ward, C. A. Hunter and N. H. Williams, *Acc. Chem. Res.*, 2018, **51**, 2073; (*b*) M. D. Ward, *Chem. Commun.*, 2024, **60**, 10464; (*c*) I. S. Tidmarsh, T. B. Faust, H. Adams, L. P. Harding, L. Russo, W. Clegg and M. D. Ward, *J. Am. Chem. Soc.*, 2008, **130**, 15167.

3 (*a*) W. Cullen, M. C. Misuraca, C. A. Hunter, N. H. Williams and M. D. Ward, *Nat. Chem.*, 2016, **8**, 231; (*b*) C. Mozaceanu, C. G. P. Taylor, J. R. Piper, S. P. Argent and M. D. Ward, *Chemistry*, 2020, **2**, 22; (*c*) W. Cullen, A. J. Metherell, A. B. Wragg, C. G. P. Taylor, N. H. Williams and M. D. Ward, *J. Am. Chem. Soc.*, 2018, **140**, 2821; (*d*) J. C. Doratt, C. G. P. Taylor, R. J. Young, A. B. Solea, D. R. Turner, G. H. Dennison, M. D. Ward and K. L. Tuck, *Chem. – Eur. J.*, 2024, **30**, e202400501; (*e*) M. D. Ludden, C. G. P. Taylor, M. B. Tipping, J. S. Train, N. H. Williams, J. C. Dorratt, K. L. Tuck and M. D. Ward, *Chem. Sci.*, 2021, **12**, 14781.

4 (*a*) C. G. P. Taylor, A. J. Metherell, S. P. Argent, F. M. Ashour, N. H. Williams and M. D. Ward, *Chem. – Eur. J.*, 2020, **26**, 3065; (*b*) A. B. Solea, B. Sudittapong, C. G. P. Taylor and M. D. Ward, *Dalton Trans.*, 2022, **51**, 11277.

5 (*a*) X. Zhang, B. Sudittapong and M. D. Ward, *Inorg. Chem. Front.*, 2023, **10**, 1270; (*b*) A. B. Solea and M. D. Ward, *Dalton Trans.*, 2023, **52**, 4456.

6 (*a*) A. D. Bokare and W. Choi, *J. Hazard. Mater.*, 2014, **275**, 121; (*b*) P. Kumari and A. Kumar, *Res. Surf. Interfaces*, 2023, **11**, 100122; (*c*) D. Ma, H. Yi, C. Lai, X. Liu, X. Huo, Z. An, L. Li, Y. Fu, B. Li, M. Zhang, L. Qin, S. Liu and L. Yang, *Chemosphere*, 2021, **275**, 130104; (*d*) Y. R. Wang and W. Chu, *J. Hazard. Mater.*, 2011, **186**, 1455.

7 (*a*) J. Wang and S. Wang, *Chem. Eng. J.*, 2018, **334**, 1502; (*b*) F. Ghanbari and M. Moradi, *Chem. Eng. J.*, 2017, **310**, 41; (*c*) X. Zheng, X. Niu, D. Zhang, M. Lv, X. Ye, J. Ma, Z. Lin and M. Fu, *Chem. Eng. J.*, 2022, **429**, 132323; (*d*) J. Lee, U. von Gunten and J.-H. Kim, *Environ. Sci. Technol.*, 2020, **54**, 3064.

8 (*a*) S. P. Argent, F. C. Jackson, H. M. Chan, S. Meyrick, C. G. P. Taylor, T. K. Ronson, J. P. Rourke and M. D. Ward, *Chem. Sci.*, 2020, **11**, 10167; (*b*) N. K. Al-Rasbi, I. S. Tidmarsh, S. P. Argent, H. Adams, L. P. Harding and M. D. Ward, *J. Am. Chem. Soc.*, 2008, **130**, 11641.

9 M. D. Ludden and M. D. Ward, *Dalton Trans.*, 2021, **50**, 2782.

10 (*a*) R. Al-Tohamy, S. S. Ali, F. Li, K. M. Okasha, Y. A.-G. Mahmoud, T. Elsamahy, H. Jiao, Y. Fu and J. Sun, *Ecotoxicol. Environ. Saf.*, 2022, **231**, 113160; (*b*) L. D. Ardila-Leal, R. A. Poutou-Piñales, A. M. Pedroza-Rodríguez and B. E. Quevedo-Hidalgo, *Molecules*, 2021, **26**, 3813;

(*c*) P. Verma and S. K. Samanta, *Environ. Chem. Lett.*, 2018, **16**, 969.

11 (*a*) A. V. Mohod, M. Momotko, N. S. Shah, M. Marchel, M. Imran, L. Kong and G. Boczkaj, *Water Res. Ind.*, 2023, **30**, 100220; (*b*) P. Zawadki and M. Deska, *Catalysts*, 2021, **11**, 974; (*c*) A. Iqbal, A. Yusaf, M. Usman, T. H. Bokhari and A. Mansha, *Int. J. Environ. Anal. Chem.*, 2024, **104**, 5503.

12 (*a*) J. S. Fleming, K. L. V. Mann, C.-A. Carraz, E. Psillakis, J. C. Jeffery, J. A. McCleverty and M. D. Ward, *Angew. Chem., Int. Ed.*, 1998, **37**, 1279; (*b*) I. S. Tidmarsh, B. F. Taylor, M. J. Hardie, L. Russo, W. Clegg and M. D. Ward, *New J. Chem.*, 2009, **33**, 366.

13 (*a*) M. Dakkach, M. I. Lopez, I. Romero, M. Rodriguez, A. Atlamsani, T. Parella, X. Fontrodona and A. Llobet, *Inorg. Chem.*, 2010, **49**, 7072; (*b*) D. Sykes, S. C. Parker, I. V. Sazanovich, A. Stephenson, J. A. Weinstein and M. D. Ward, *Inorg. Chem.*, 2013, **52**, 10500.

14 (*a*) A. J. Metherell, W. Cullen, A. Stephenson, C. A. Hunter and M. D. Ward, *Dalton Trans.*, 2014, **43**, 71; (*b*) A. J. Metherell and M. D. Ward, *Dalton Trans.*, 2016, **45**, 16096.

15 M. B. Tipping, J. M. Woolley, J. R. Williams and M. D. Ward, *Chem. – Eur. J.*, 2025, **31**, e202404647.

16 M. D. Ludden, C. G. P. Taylor and M. D. Ward, *Chem. Sci.*, 2021, **12**, 12640.

17 Bindfit: P. Thordarson, **https://supramolecular.org**(accessed 20/5/25).

18 (*a*) M. Schmalzbauer, M. Marcon and B. Konig, *Angew. Chem., Int. Ed.*, 2021, **60**, 6270; (*b*) X.-F. Zhang, I. Zhang and L. Liu, *Photochem. Photobiol.*, 2010, **86**, 492.

19 F. S. T. Khan, A. L. Waldbusser, M. C. Carrasco, H. Pourhadi and S. Hematian, *Dalton Trans.*, 2021, **50**, 7433.

20 (*a*) X. Jing, C. He, L. Zhao and C. Duan, *Acc. Chem. Res.*, 2019, **52**, 100; (*b*) R. Ham, C. J. Nielsen, S. Pullen and J. N. H. Reek, *Chem. Rev.*, 2023, **123**, 5225; (*c*) S. Gaikwad, A. Bhattacharjee and E. Elacqua, *Chem. – Eur. J.*, 2025, **31**, e202404699.

21 (*a*) H. J. Lim, D. J. Kim, K. Rigby, W. Chen, H. Xu, X. Wu and J.-H. Kim, *Environ. Sci. Technol.*, 2023, **57**, 19054; (*b*) X. Xia, F. Zhu, J. Li, H. Yang, L. Wei, Q. Li, J. Jiang, G. Zhang and Q. Zhao, *Front. Chem.*, 2020, **8**, 592056.